

Dijet mass up to four-loops with(out) k_t clustering

K. Khelifa-Kerfa^{a,1}

¹Department of Physics, Faculty of Science and Technology
Relizane University, Relizane 48000, Algeria

Abstract We compute the invariant mass of dijets produced in e^+e^- annihilation processes up to four-loops in perturbation theory for both anti- k_t and k_t jet algorithms. The calculations, performed within the eikonal approximation and employing strong-energy ordering, capture the full analytic structure of the leading Abelian and non-Abelian non-global logarithms, including full colour and jet-radius dependence. We evaluate the significance of these logarithms and the convergence of the four-loop perturbative expansion by comparing with all-orders numerical results.

PACS 12.38.Bx · 12.38.Cy · 13.87.-Ce · 13.85.Fb

Keywords QCD · Jets · Jet algorithms · Resummation

1 Introduction

In high-energy particle collisions, such as e^+e^- annihilation into dijets, jets are central to understanding the underlying dynamics of QCD. Jets, which represent collimated sprays of final-state hadrons produced from the fragmentation of quarks and gluons, are indispensable tools for probing QCD in both perturbative and non-perturbative regimes. They are typically reconstructed using jet algorithms, such as the anti- k_t [1] and k_t [2, 3] algorithms, both of which have substantial implications for theoretical calculations and experimental measurements.

In the perturbative QCD context, calculations of jet shapes and substructure present considerable complexity, even in relatively simple leptonic processes. This is due to the presence of multiple energy scales that induce large logarithms, which spoil the perturbative expansion and necessitate resummation. These logarithms fall into two primary categories: global (abelian) logarithms (GLs), arising in QCD observables defined over the entire phase space, and non-global (non-abelian) logarithms (NGLs) [4, 5], which emerge

in observables confined to a restricted phase space region. While global observables have been analytically computed up to next-to-next-to-leading order (NNLO) (see, e.g., [6, 7]) and (analytically and/or numerically) resummed to next-to-next-to-leading logarithmic (NNLL) accuracy for general observables [8]—and even to N³LL for certain cases [9–15]—non-global observables have, until recently, been resummed only up to NLL, numerically and within the large- N_c limit [4, 5, 16]. Recent advancements have improved this to include finite- N_c effects at NLL [17–20] as well as NNLL resummation in the large- N_c limit [21, 22].

Fixed-order (FO) calculations of jet shapes and substructure are essential complements to all-orders resummations. FO methods typically offer analytical insights, enhancing understanding of non-global observable distributions at high energy scales. They also incorporate higher-order corrections that improve precision by accounting for effects like multiple emissions, interference terms, and virtual corrections, which may not be fully captured by resummation. Combining FO and all-orders results enables more reliable predictions across a wider spectrum of the observable, providing refined theoretical uncertainties. Since their initial computation at two-loops for the hemisphere mass [4], NGLs have been studied for various observables (e.g., [5, 23–29]). For certain cases, higher-order terms have been computed up to twelve-loops at large- N_c [30–32], with recent progress, at finite- N_c , extending (fully) to four-loops and (partially) to five-loops for a range of observables in processes such as e^+e^- annihilation [33, 34] and Higgs/vector boson plus jet production [35].

The aforementioned calculations were primarily carried out for the anti- k_t jet algorithm. When alternative clustering algorithms, such as the k_t algorithm, are employed, these calculations become increasingly intricate and complex. It was first observed in [36, 37] for the interjet energy flow that the magnitude of NGLs diminishes due to the k_t algorithm's

^ae-mail: kamel.khelifakerfa@univ-relizane.dz

non-linear clustering condition, which influences the secondary correlated emissions responsible for NGLs. Furthermore, [38] later demonstrated that k_T clustering leads to a new hierarchy of large logarithmic terms for abelian primary emissions, termed clustering logarithms (CLs) (or equivalently abelian NGLs). Both of these effects have since been validated through calculations for various non-global observables (see, e.g., [25–27, 29, 39–42]). Fixed-order (FO) calculations of CLs beyond the leading two-loops level were first performed in [39] (up to four-loops) for interjet energy flow and subsequently for the single-jet-mass [43] and azimuthal decorrelation (up to three-loops) [34], all in e^+e^- annihilation processes and at the leading-logarithmic level, with the exception of Ref. [27], which calculated next-to-leading logarithms at two-loops. No comparable calculations currently exist for hadron-hadron collisions, an area to be addressed in a forthcoming paper [44]. On another front, all-orders resummation of leading CLs exists only in numerical form, as implemented in the Monte Carlo (MC) code of [4] (limited to the k_T algorithm), and more recently within the framework of Soft and Collinear Effective Theory (SCET) for both k_T and Cambridge/Aachen [45, 46] clustering algorithms [47].

In this paper, we examine the leptonic process of e^+e^- annihilation into two final-state jets in the threshold limit, where the jets are produced back-to-back. We compute the invariant mass (squared) of the dijet system within the framework of eikonal theory, imposing a strong energy-ordering condition on the emitted soft gluons. This approach allows us to utilise the squared eikonal amplitudes derived in [48]. The calculations are performed for both the anti- k_T and k_T jet algorithms. Our observable is closely related to that studied in [26, 27, 49], with the key difference that we impose no energy cutoff on the soft activity outside the two jets, thereby eliminating any logarithms associated with this cutoff. Furthermore, this paper extends the calculations of these prior studies, which were limited to two-loops, up to four-loops.

For anti- k_T clustering, our calculations closely follow those conducted for the hemisphere mass observable [33]. In the case of the dijet mass, however, there is a dependence on the jet-radius R , affecting both the argument of the large non-global logarithms and the coefficients that multiply them at each order in the perturbative expansion. Calculations are carried out analytically wherever feasible; otherwise, numerical approximations are employed. Notably, in the anti- k_T algorithm, no clustering logarithms arise, as this clustering algorithm tends to produce more collimated jets (similar to cone algorithms), rendering it less sensitive to soft radiation located far from the jet axis.

The k_T jet algorithm, by contrast, is more inclusive, clustering soft radiation earlier in the recombination sequence. This leads to a reorganisation of the final-state partons, altering the original phase space and resulting in the previously

mentioned effects: a reduction in the size of NGLs (through the clustering of small-angle secondary radiation) and the emergence of CLs (due to the clustering of soft radiation into the jet, thereby increasing its effective size [47]). Unlike CLs, which were computed up to four-loops some time ago, as discussed previously, NGLs in k_T clustering have been computed only up to two-loops. However, very recently, the three-loop coefficient was successfully determined for the dijet azimuthal decorrelation observable in e^+e^- annihilation [34]. In this work, we employ the recently derived master formula (Eq. (21)) from Ref. [50] to compute NGLs up to four-loops for the k_T jet algorithm. This formula systematises and generalises the calculation for any non-global observable in both lepton and hadron processes. Due to the complex phase space factors in the relevant integrals, these calculations are carried out numerically; nevertheless, they include full dependence on both jet-radius and colour.

We compare the two-loops distributions for both anti- k_T and k_T with the fixed-order next-to-leading order (NLO) Monte Carlo (MC) program `event2` [51], interfaced with the `FastJet` package [52], and find consistency within the precision of our calculations. Furthermore, a pattern of exponentiation for NGLs and CLs emerges clearly up to four-loops. It is instructive to separately compare the exponentiated NGLs and CLs to the output of the MC code from [4] to examine the convergence of the perturbative series. Our results indicate that the inclusion of higher-order terms expands the overlap range between the analytical exponentiation and the numerical results. Notably, while a comparison with all-orders resummation at finite colour would be preferable, such resummation is currently only available, in e^+e^- processes, for the hemisphere mass observable [17, 18]. We also derive the all-orders resummed formula, incorporating the primary Sudakov form factor, the exponential of NGLs, and the exponential of CLs (in the k_T clustering case), to evaluate the significance of the latter two effects in phenomenological studies. Our findings confirm previous conclusions, specifically: (a) NGLs can reduce the Sudakov form factor by up to 25% near the peak of the distribution, and (b) the CLs form factor counteracts the NGLs effect, moderating the Sudakov factor reduction to approximately 5%, and even down to only 2% for larger jet-radii.

This paper is organised as follows. In Sec. 2, we present the definitions of the various components, including the jet shape observable and the jet algorithms. Sec. 3 is dedicated to detailed calculations of the dijet mass at one-, two-, three- and four-loops in the anti- k_T algorithm, with comparisons to `event2` shown in the same section. The corresponding calculations for the k_T algorithm are presented in Sec. 4. Sec. 5 presents the all-orders analytical calculations, including a quantification of the contributions of NGLs and CLs to the full resummation. In the same section, we compare the exponentiated NGLs and CLs up to four-loops with the numerical

distribution from the MC code of [4], assessing the effect of higher-order terms. Finally, we summarise our findings and outline future directions in Sec. 6.

2 Definitions

Consider the simple QCD process of e^+e^- annihilation into dijets that are produced, in the threshold limit, back-to-back in the lab frame. At the partonic level, we may write:

$$e^+ + e^- \rightarrow q(p_a) + \bar{q}(p_b) + g_1(k_1) + \dots + g_n(k_n), \quad (1)$$

where the quantities in parentheses denote the four-momenta of the respective partons (the quark q , the anti-quark \bar{q} , and gluons $g_i, i = 1, \dots, n$). These can be expressed in polar parametrisation (spherical coordinates) as follows:

$$\begin{aligned} p_a &= \frac{Q}{2} (1, 0, 0, 1), \\ p_b &= \frac{Q}{2} (1, 0, 0, -1), \\ k_i &= \omega_i (1, s_i \cos \phi_i, s_i \sin \phi_i, c_i), \end{aligned} \quad (2)$$

where $c_i \equiv \cos \theta_i$ and $s_i \equiv \sin \theta_i$, with θ_i and ϕ_i being the polar and azimuthal angles of the i^{th} gluon. The energy scales Q and ω_i represent the hard scale of the process and the energy of the i^{th} soft gluon g_i , respectively. All partons are assumed to be massless. At single-logarithmic (SL) accuracy—i.e., retaining logarithmic terms up to $\alpha_s^n L^{2n-2}$ in the perturbative expansion of the non-global jet-mass observable—recoil effects can safely be neglected. Additionally, at SL accuracy, we work within the soft eikonal approximation and impose strong energy-ordering of the soft gluons: $Q \gg \omega_1 \gg \omega_2 \gg \dots \gg \omega_n$. These latter two approximations greatly simplify calculations at higher orders in the perturbative series.

The normalised invariant mass (squared) of the dijets, ρ , is defined as:

$$\rho = \rho_R + \rho_L, \quad (3)$$

where

$$\begin{aligned} \rho_R &= \frac{4m_R^2}{Q^2} = \frac{4}{Q^2} \left(p_a + \sum_{i \in j_R} k_i \right)^2 = \sum_{i \in j_R} \rho_{R,i} + \mathcal{O} \left(\frac{\omega^2}{Q^2} \right) \\ \rho_{R,i} &= 8 \frac{p_a \cdot k_i}{Q^2} = \frac{4\omega_i}{Q} (1 - c_i) = 2x_i (1 - c_i), \end{aligned} \quad (4)$$

where $x_i = 2\omega_i/Q$ is the energy fraction of the i^{th} gluon, and the sum runs over all soft gluons that are clustered by the jet algorithm into the right (quark-initiated) jet j_R . An identical expression holds for the normalised invariant mass of the left (anti-quark-initiated) jet j_L . In the above definition of ρ_R , terms proportional to ω^2/Q^2 are neglected in the soft limit.

The anti- k_t and k_t jet algorithms can be defined following the framework of Ref. [52]. In this framework, both algorithms are members of a more general class of sequential recombination algorithms known as the ‘‘generalised k_t algorithm,’’ which depends on a continuous parameter p . Specifically, this algorithm proceeds as follows:

1. For each pair in the initial list of final-state particles, define the two distance measures:

$$\begin{aligned} d_{ij} &= \min \left(E_i^{2p}, E_j^{2p} \right) \frac{1 - \cos \theta_{ij}}{1 - \cos R}, \\ d_{iB} &= E_i^{2p}, \end{aligned} \quad (5)$$

where E_i is the energy of the i^{th} particle, R is the jet-radius parameter, and $\cos \theta_{ij} = c_i c_j + s_i s_j \cos \phi_{ij}$ with $\phi_{ij} = \phi_i - \phi_j$. The anti- k_t and k_t jet algorithms correspond to values of the parameter $p = -1$ and $p = 1$, respectively. Here, the subscript B in d_{iB} refers to the beam direction.

2. Let d_{\min} be the minimum of all d_{ij} and d_{iB} . If d_{\min} corresponds to a d_{ij} , then particles i and j are merged into a single pseudo-jet, with their momenta summed up (in the E -scheme recombination). If d_{\min} corresponds to a d_{iB} , then particle i is declared a final (inclusive) jet and removed from the list of final-state particles.
3. Steps 1 and 2 are repeated until no particles remain in the list.

Notice that for the anti- k_t jet algorithm ($p = -1$), clustering proceeds with the harder particles first, as they minimise the energy-reciprocal measure E^{-2} . If no other particles are within a distance R from a given hard particle, then that particle forms an inclusive jet. Consequently, hard, well-separated jets appear as circular regions on the θ - ϕ plane with radius R . This approach offers a simple, infrared- and collinear-safe alternative to cone-like algorithms for e^+e^- collisions [53].

In contrast, the k_t jet algorithm ($p = 1$) clusters the softest particles first, as they have the minimum energies E^2 . Two soft particles are merged if their distances satisfy:

$$1 - \cos \theta_{ij} < 1 - \cos R. \quad (6)$$

Thus, a soft gluon initially located outside a jet (perhaps during the early stages of the k_t jet algorithm) can later be clustered with a harder gluon already inside the jet. This results in the soft gluon being ‘‘dragged’’ into the jet, where it contributes to the jet-mass. Such behaviour is absent in the anti- k_t algorithm and demonstrates that clustering among soft gluons can significantly impact the jet-mass distribution. It also highlights that clustering among soft gluons is inherently complex, implying that their contribution to the jet-mass observable will be equally intricate. This observation will be further substantiated later in the text.

In this paper, we focus on calculating the jet-mass integrated cross-section (or, equivalently, the jet-mass cumulant), $\Sigma(\rho)$, defined as:

$$\Sigma(\rho) = \int \frac{1}{\sigma_0} \frac{d\sigma}{d\rho} \Theta[\rho - \rho(k_1, \dots, k_n)] \Xi(k_1, \dots, k_n) d\rho, \quad (7)$$

where σ_0 denotes the Born cross-section, and $d\sigma/d\rho$ represents the differential cross-section in the normalised jet-mass $\rho(k_1, \dots, k_n)$, which is restricted to be less than a threshold ρ . The clustering function $\Xi(k_1, \dots, k_n)$ arises from the application of the chosen jet algorithm and limits the final-state phase space to only include gluonic configurations that contribute to the jet-mass. The fixed-order perturbative expansion of this integrated cross-section can be expressed as:

$$\Sigma(\rho) = 1 + \Sigma_1(\rho) + \Sigma_2(\rho) + \dots, \quad (8)$$

where the m^{th} term in the expansion is given by:

$$\Sigma_m(\rho) = \sum_X \int_{x_1 > x_2 > \dots > x_m} \prod_{i=1}^m d\Phi_i \times \times \hat{\mathcal{U}}_m \mathcal{W}_{1\dots m}^X \Xi_m(k_1, \dots, k_m), \quad (9)$$

where the phase-space factor for the emission of the i^{th} soft gluon is given by:

$$d\Phi_i = \bar{\alpha}_s \frac{dx_i}{x_i} dc_i \frac{d\phi_i}{2\pi}, \quad (10)$$

with $\bar{\alpha}_s = \alpha_s/\pi$. The eikonal amplitude squared for the emission of m soft, energy-ordered gluons in the configuration X , normalised to the Born cross-section, $\mathcal{W}_{1\dots m}^X$, has been defined and extensively discussed in Ref. [48] for e^+e^- processes. Each gluon may be real (R) or virtual (V), and X denotes a possible configuration of m such gluons. For example, X could be $\{RR\dots V\}$, where g_1 and g_2 are real, \dots , and g_m is virtual. The summation in Eq. (9) runs over all possible configurations X at each order in the perturbative series. Explicit formulae for the eikonal amplitudes squared up to four-loops are provided in the aforementioned reference [48].

The measurement operator at the m^{th} -order, $\hat{\mathcal{U}}_m$, acts on a given eikonal amplitude squared to ensure that only gluon configurations for which the jet-mass observable is less than ρ contribute non-trivially to the integrated cross-section $\Sigma(\rho)$. All other configurations are set to zero. This operator was first introduced by Schwartz and Zhu in [30] and later utilised in [33] for calculating the hemisphere mass observable up to four-loops in the anti- k_t algorithm. Interested readers are referred to these references for comprehensive details. Notably, in both the anti- k_t and k_t algorithms, it factorises as follows [30, 33, 50]:

$$\hat{\mathcal{U}}_m = \prod_{i=1}^m \hat{u}_i, \quad (11)$$

where the measurement operator for the i^{th} emission reads:

$$\hat{u}_i = \Theta_i^V + \Theta_i^R \left[\Theta_i^{\text{out}} + \Theta_i^{\text{in}} \Theta(\rho - \rho_i) \right] = 1 - \Theta_i^R \Theta_i^{\text{in}} \Theta_i^\rho, \quad (12)$$

with the step-function $\Theta_i^{V(R)}$ equals to one if gluon g_i is virtual (real) and zero otherwise. Additionally, $\Theta_i^{\text{out(in)}}$ is equal to one if gluon g_i is outside (inside) either jet j_R or j_L (after applying the jet algorithm) and zero otherwise. The jet-mass step-function is defined as $\Theta_i^\rho \equiv \Theta(\rho_i - \rho)$. Note that $\Theta_i^R + \Theta_i^V = 1$ and $\Theta_i^{\text{in}} + \Theta_i^{\text{out}} = 1$.

We begin by presenting fixed-order calculations in the anti- k_t jet algorithm in the next section, Sec. 3, and then proceed to the k_t jet algorithm in Sec. 4.

3 Fixed-order calculations in anti- k_t

3.1 One- and two-loops

At one-loop, the quark–anti-quark hard antenna emits a single soft gluon k_1 , which can be either real or virtual. The corresponding eikonal amplitudes squared are thus [48]:

$$\mathcal{W}_1^R = C_F w_{ab}^1, \quad \mathcal{W}_1^V = -\mathcal{W}_1^R, \quad (13)$$

where the Casimir colour factor $C_F = (N_c^2 - 1)/2N_c$, with N_c being the number of colours in the fundamental representation, and the one-loop antenna function reads:

$$w_{ab}^k = \omega_k^2 \frac{(p_a \cdot p_b)}{(p_a \cdot k)(k \cdot p_b)} = \omega_k^2 \frac{(ab)}{(ak)(kb)}. \quad (14)$$

Summing over these two gluon configurations, we find for the integrand in (9)

$$\sum_X \hat{u}_1 \mathcal{W}_1^X = \hat{u}_1 \mathcal{W}_1^R + \hat{u}_1 \mathcal{W}_1^V = -\Theta_1^\rho \Theta_1^{\text{in}} \mathcal{W}_1^R, \quad (15)$$

where we have applied the one-loop measurement operator \hat{u}_1 from (12) on the real and virtual eikonal amplitudes squared to obtain the last equality. We note that at one-loop order, there are no differences between the various jet algorithms, and they all yield the same results. From the above equation (15), it is straightforward to see that the anti- k_t clustering function is, at one-loop, simply equal to:

$$\Xi_1^{\text{ak}_t}(k_1) = \Theta_1^{\text{in}}, \quad (16)$$

where ak_t is a shorthand for the anti- k_t jet algorithm. Substituting (15) into the formula for the cumulant (9) at one-loop gives:

$$\begin{aligned} \Sigma_1^{\text{ak}_t}(\rho) &= - \int d\Phi_1 \Theta_1^\rho \Theta_1^{\text{in}} \mathcal{W}_1^R, \\ &= -C_F \bar{\alpha}_s \int_0^1 \frac{dx_1}{x_1} \left(\int_{-1}^{-c_R} \Theta[2x_1(1+c_1) - \rho] + \right. \\ &\quad \left. + \int_{c_R}^1 \Theta[2x_1(1-c_1) - \rho] \right) dc_1 \int_0^{2\pi} \frac{d\phi_1}{2\pi} w_{ab}^1, \end{aligned} \quad (17)$$

where $c_R \equiv \cos R$, and Θ_1^{in} has been replaced by the expression $\Theta(1 - c_1, c_1 - c_R) + \Theta(1 + c_1, -c_R - c_1)$. The one-loop antenna function w_{ab}^1 is given by $2/(1 - c_1^2)$. To capture the hard-collinear contribution to the distribution, we replace $1/x_1$ with $(1 + (1 - x_1)^2)/2x_1$. Performing the integration up to SL accuracy, we obtain:

$$\Sigma_1^{\text{akt}}(\rho) = -C_F \bar{\alpha}_s \left[L^2 + \left(\frac{3}{2} - 2 \ln \frac{1 - c_R}{1 + c_R} \right) L \right] \equiv \Sigma_1^{\text{P}}(\rho), \quad (18)$$

where $L = \ln(1/\rho)$ and the superscript P refers to primary emissions. That is, the leading logarithms in the dijet mass distribution are entirely captured by primary emissions off the hard $q\bar{q}$ pair. They originate from soft and collinear singularities of the corresponding part of the eikonal amplitude squared. The all-orders resummation of these leading double logarithms, which form the Sudakov form factor, has been known for decades as a simple exponential of the one-loop result (18). Figure 1 shows the difference between the analytical and exact (`event2`) differential distributions at leading order for a jet-radius $R = 0.7$:

$$r_{\text{LO}}(L) = \frac{d\sigma_{\text{LO}}^{\text{event2}}}{d\tilde{L}} - \frac{d\Sigma_1^{\text{akt}}}{d\tilde{L}}, \quad (19)$$

where $\tilde{L} = \ln \rho = -L$ and the factor $(\alpha_s/2\pi)$ is omitted¹. As expected, the difference tends to zero at large logarithms. The cutoff in the `event2` distribution corresponds to the maximum value of the dijet mass observable, given by [26, 27]:

$$\rho_{\text{max}} = \frac{8}{R^2} \left(1 - \sqrt{1 - R^2/4} \right) - 1. \quad (20)$$

We emphasise again that Fig. 1 would be identical for all jet

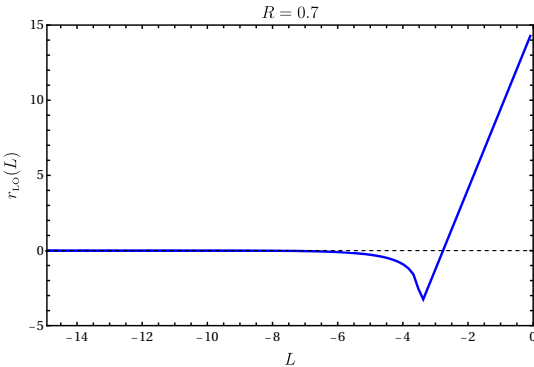


Fig. 1 Comparisons between the analytical and `event2` differential distributions for the dijet mass observable at one-loop.

¹The differential distributions in `event2` exclude the prefactor $(\alpha_s/2\pi)$ and the Casimir colour factors, at both leading- and next-to-leading order.

algorithms since, as mentioned above, they operate equivalently at this order. It is also worth noting that the result in (18) matches that found in [26, 27], corresponding to the τ_{E_0} part of the distribution with $1 - c_R = 2R_s$.

For the emission of two soft, energy-ordered gluons, k_1 and k_2 , the sum over all possible gluon configurations (9) at two-loop order is given by [33, 50]:

$$\begin{aligned} \sum_X \hat{\mathcal{W}}_2^X \mathcal{W}_{12}^X &= \hat{u}_1 \hat{u}_2 (\mathcal{W}_{12}^{\text{RR}} + \mathcal{W}_{12}^{\text{RV}} + \mathcal{W}_{12}^{\text{VR}} + \mathcal{W}_{12}^{\text{VV}}), \\ &= -\Theta_1^{\text{P}} \Theta_2^{\text{P}} \Theta_2^{\text{in}} [\mathcal{W}_{12}^{\text{VR}} + \Theta_1^{\text{out}} \mathcal{W}_{12}^{\text{RR}}], \end{aligned} \quad (21)$$

where the second equality arises from applying the measurement operators of the first and second emissions on the various eikonal amplitudes squared. Note that other gluon configurations either do not produce real-virtual mis-cancellations (and thus no large logarithms) or do produce large logarithms but are subleading. For instance, configurations where the harder gluon k_1 is inside the left-jet j_L and radiates the softer gluon k_2 inside the right-jet j_R . Although the softer gluon k_2 contributes to the mass of j_R , this contribution is subleading because k_1 , being inside j_L , is vetoed. Such scenarios are discussed in detail in Refs. [26, 27].

Using the relation $\Theta_1^{\text{in}} + \Theta_1^{\text{out}} = 1$ and the explicit expressions of the eikonal amplitudes squared [48], we can further simplify the above equation to:

$$\sum_X \hat{\mathcal{W}}_2^X \mathcal{W}_{12}^X = -\Theta_1^{\text{P}} \Theta_2^{\text{P}} \left[-\Theta_1^{\text{in}} \Theta_2^{\text{in}} \mathcal{W}_1^{\text{R}} \mathcal{W}_2^{\text{R}} + \Theta_1^{\text{out}} \Theta_2^{\text{in}} \overline{\mathcal{W}}_{12}^{\text{RR}} \right], \quad (22)$$

where the one-loop eikonal amplitude squared, \mathcal{W}_i^{R} , is given above, and the *irreducible* part of the two-loop eikonal amplitude squared, $\overline{\mathcal{W}}_{12}^{\text{RR}}$, reads [7]:

$$\overline{\mathcal{W}}_{12}^{\text{RR}} = \frac{1}{2} C_F C_A \mathcal{A}_{ab}^{12}, \quad \mathcal{A}_{ab}^{ij} = w_{ab}^i \left(w_{ai}^j + w_{ib}^j - w_{ab}^j \right). \quad (23)$$

The term \mathcal{A}_{ab}^{ij} is known as the two-loops antenna function. From Eq. (22) we can see that the two-loops clustering function for primary emissions is simply the product of the corresponding one-loop functions (16), whereas, for secondary correlated emissions, it is given by:

$$\Xi_2^{\text{akt}}(k_1, k_2) = \Theta_1^{\text{out}} \Theta_2^{\text{in}}. \quad (24)$$

Substituting Eq. (22) into the expression of the cumulant (9) at two-loops, we obtain:

$$\Sigma_2(\rho) = \int_{1_{\text{in}}} \int_{2_{\text{in}}} \mathcal{W}_1^{\text{R}} \mathcal{W}_2^{\text{R}} - \int_{1_{\text{out}}} \int_{2_{\text{in}}} \overline{\mathcal{W}}_{12}^{\text{RR}}, \quad (25)$$

where we have introduced the shorthand notation:

$$\int_{i_y} = \int d\Phi_i \Theta_i^{\text{P}} \Theta_i^y, \quad y \in \{\text{in}, \text{out}\}, \quad (26)$$

and strong-energy ordering $x_1 > x_2$ is implied. The first part on the right-hand side (rhs) of Eq. (25) is the two-loop term in the series expansion of the Sudakov form factor:

$$\int_{1_{\text{in}}} \int_{2_{\text{in}}} \mathcal{W}_1^R \mathcal{W}_2^R = \frac{1}{2!} (\Sigma_1^P)^2. \quad (27)$$

The second part on the rhs of Eq. (25) represents the first pure NGLs contribution to the dijet mass distribution. At SL accuracy, the energy integrals factorise out, resulting in a logarithm $L^2/2!$ (see, for instance, [33] for details). The remaining integral can be cast as:

$$\Sigma_{2,\text{ng}}^{\text{akt}}(\rho) = -2\bar{\alpha}_s^2 \frac{L^2}{2!} C_{\text{F}} C_{\text{A}} \mathcal{G}_2^{\text{akt}}(R), \quad (28)$$

where the factor of 2 accounts for both jets, j_{R} and j_{L} , and the two-loopsNGLs coefficient $\mathcal{G}_2^{\text{akt}}(R)$ is given by:

$$\mathcal{G}_2^{\text{akt}}(R) = \frac{1}{2} \int_{1_{\text{out}}} \int_{2_{\text{in}}} \mathcal{A}_{ab}^{12} = \zeta_2 - \text{Li}_2 \left[\left(\frac{1-c_R}{1+c_R} \right)^2 \right]. \quad (29)$$

This analytical formula is equivalent to the result in [5, 26, 27, 36], expressed in terms of the rapidity gap $\Delta\eta$, which is related to the jet-radius R by $\Delta\eta = -\ln(1-c_R)/(1+c_R)$. Figure 2 shows a plot of $\mathcal{G}_2(R)$ as a function of R for both anti- k_t and k_t algorithms; we defer discussion of these curves to Sec. 4.1. In the limit $R \rightarrow 0$, one recovers the hemisphere mass result [4, 33]: $\mathcal{G}_2^{\text{akt}} = \zeta_2$.

In Figure 3, we plot the difference between the analytical and event2 differential distributions at two-loops for a jet-radius $R = 0.7$ and for all three colour channels; C_{F}^2 , $C_{\text{F}} C_{\text{A}}$ and $C_{\text{F}} T_f n_f$:

$$r^{\text{NLO}}(L) = \frac{d\sigma^{\text{event2}}}{d\tilde{L}} - \frac{d\Sigma_2^{\text{akt}}}{d\tilde{L}}. \quad (30)$$

The details of the analytical distribution are found in Appendices A, B, and C of Ref. [26]². We observe that all three curves tend to a constant at large values of \tilde{L} , indicating agreement up to $\bar{\alpha}_s^2 L$ in the differential distribution.

3.2 Three-loops

In the case of the emission of three soft, energy-ordered gluons, k_1 , k_2 , and k_3 , the sum over all possible gluon configurations yields the formula [26, 50]:

$$\begin{aligned} \sum_X \hat{\mathcal{W}}_3^X \mathcal{W}_{123}^X &= -\Theta_1^P \Theta_2^P \Theta_3^P \Theta_3^{\text{in}} \left[\mathcal{W}_{123}^{\text{VVR}} + \Theta_1^{\text{out}} \mathcal{W}_{123}^{\text{RVR}} + \right. \\ &\quad \left. + \Theta_2^{\text{out}} \mathcal{W}_{123}^{\text{VRR}} + \Theta_1^{\text{out}} \Theta_2^{\text{out}} \mathcal{W}_{123}^{\text{RRR}} \right]. \end{aligned} \quad (31)$$

²The distribution of the dijet mass observable may be derived from the jet-thrust τ_{E_0} of [26] up to two-loops by setting $\log(2E_0/Q)$ in [26] to zero.

Following the procedure outlined above for the two-loops calculations and substituting the expressions for the three-loop eikonal amplitudes squared from Ref. [48], we find that the cumulant (9) at this order ($m = 3$) is given by:

$$\begin{aligned} \Sigma_3^{\text{akt}}(\rho) &= - \int_{1_{\text{in}}} \int_{2_{\text{in}}} \int_{3_{\text{in}}} \mathcal{W}_1^R \mathcal{W}_2^R \mathcal{W}_3^R + \int_{2_{\text{in}}} \mathcal{W}_2^R \int_{1_{\text{out}}} \int_{3_{\text{in}}} \overline{\mathcal{W}}_{13}^{\text{RR}} \\ &\quad + \int_{3_{\text{in}}} \mathcal{W}_3^R \int_{1_{\text{out}}} \int_{2_{\text{in}}} \overline{\mathcal{W}}_{12}^{\text{RR}} + \int_{1_{\text{in}}} \mathcal{W}_1^R \int_{2_{\text{out}}} \int_{3_{\text{in}}} \overline{\mathcal{W}}_{23}^{\text{RR}} \\ &\quad + \Sigma_{3,\text{ng}}^{\text{akt}}. \end{aligned} \quad (32)$$

The first term in the equation above is simply the three-loop term in the expansion of the Sudakov form factor; $(\Sigma_1^P)^3/3!$. The second, third, and fourth terms represent the interference terms between the one-loop primary contribution (18) and the two-loopsNGLs contribution (28), i.e., $\Sigma_1^P \times \Sigma_{2,\text{ng}}^{\text{akt}}$. The final term in Eq. (32) is the new irreducible NGLs contribution at this order, given by [26]:

$$\Sigma_{3,\text{ng}}^{\text{akt}}(\rho) = - \int_{1_{\text{out}}} \int_2 \int_{3_{\text{in}}} \left[\overline{\mathcal{W}}_{123}^{\text{RVR}} + \Theta_2^{\text{out}} \overline{\mathcal{W}}_{123}^{\text{RRR}} \right], \quad (33)$$

where the subscript 2 in the second integral denotes that gluon k_2 is neither in nor out. Note that $\int_{i_{\text{in}}} = \int_i \Theta_i^{\text{in}}$ and $\int_{i_{\text{out}}} = \int_i \Theta_i^{\text{out}}$. Using the relation $\Theta_2^{\text{in}} + \Theta_2^{\text{out}} = 1$ along with the explicit forms of the irreducible eikonal amplitudes squared, $\overline{\mathcal{W}}_{123}^{\text{RVR}}$ and $\overline{\mathcal{W}}_{123}^{\text{RRR}}$, the above NGLs contribution can be expressed as:

$$\Sigma_{3,\text{ng}}^{\text{akt}}(\rho) = +2\bar{\alpha}_s^3 \frac{L^3}{3!} C_{\text{F}} C_{\text{A}}^2 \mathcal{G}_3^{\text{akt}}(R), \quad (34)$$

where the factor of 2 accounts for both jets, and the three-loop NGLs coefficient $\mathcal{G}_3^{\text{akt}}$ is:

$$\mathcal{G}_3^{\text{akt}}(R) = \frac{1}{4} \left[\int_{1_{\text{out}}} \int_{2_{\text{in}}} \int_{3_{\text{in}}} \mathcal{A}_{ab}^{12} \mathcal{A}_{ab}^{13} - \int_{1_{\text{out}}} \int_{2_{\text{out}}} \int_{3_{\text{in}}} \mathcal{B}_{ab}^{123} \right], \quad (35)$$

with the three-loop antenna function \mathcal{B}_{ab}^{ijk} defined in Ref. [33] (Eq. (39b)). The result of this integration as a function of the jet-radius is shown in Fig. 4. It is evident from the figure that, in the limit $R \rightarrow 0$, one obtains $\mathcal{G}_3^{\text{akt}} = \zeta_3$, which aligns with the result for the hemisphere mass distribution [26].

3.3 Four-loops

For the emission of four soft, energy-ordered gluons, k_1, k_2, k_3 , and k_4 , the calculation of the dijet mass distribution follows an analogous procedure to the two- and three-loop cases. Specifically, the sum over possible gluon configurations is

given by:

$$\begin{aligned} \sum_X \hat{\mathcal{U}}_4 \mathcal{W}_{1234}^X &= - \prod_{i=1}^4 \Theta_i^p \Theta_4^{\text{in}} \left[\mathcal{W}_{1234}^{\text{VVVR}} + \Theta_1^{\text{out}} \mathcal{W}_{1234}^{\text{RVVR}} + \right. \\ &+ \Theta_2^{\text{out}} \mathcal{W}_{1234}^{\text{VRVR}} + \Theta_3^{\text{out}} \mathcal{W}_{1234}^{\text{VVR}} + \Theta_1^{\text{out}} \Theta_2^{\text{out}} \mathcal{W}_{1234}^{\text{RRVR}} + \\ &+ \Theta_1^{\text{out}} \Theta_3^{\text{out}} \mathcal{W}_{1234}^{\text{RVRR}} + \Theta_2^{\text{out}} \Theta_3^{\text{out}} \mathcal{W}_{1234}^{\text{VRRR}} + \\ &\left. + \Theta_1^{\text{out}} \Theta_2^{\text{out}} \Theta_3^{\text{out}} \mathcal{W}_{1234}^{\text{RRRR}} \right]. \end{aligned} \quad (36)$$

Substituting this expression into (9) at four loops ($m = 4$), and simplifying, we obtain the expected exponential expansion [33]:

$$\begin{aligned} \Sigma_4^{\text{ak}_t}(\rho) &= \frac{1}{4!} (\Sigma_1^p)^4 + \frac{1}{2!} (\Sigma_1^p)^2 \times \Sigma_{2,\text{ng}}^{\text{ak}_t} + \Sigma_1^p \times \Sigma_{3,\text{ng}}^{\text{ak}_t} + \\ &+ \frac{1}{2!} \left(\Sigma_{2,\text{ng}}^{\text{ak}_t} \right)^2 + \Sigma_{4,\text{ng}}^{\text{ak}_t}. \end{aligned} \quad (37)$$

The new irreducible NGLs contribution to the dijet mass distribution at this order is represented by the last term, $\Sigma_{4,\text{ng}}^{\text{ak}_t}$. Its explicit form is given by [33]:

$$\begin{aligned} \Sigma_{4,\text{ng}}^{\text{ak}_t}(\rho) &= - \int_{1_{\text{out}}} \int_{2_{\text{in}}} \int_{3_{\text{in}}} \int_{4_{\text{in}}} \left[\overline{\mathcal{W}}_{1234}^{\text{RVVR}} + \Theta_2^{\text{out}} \overline{\mathcal{W}}_{1234}^{\text{RRVR}} \right. \\ &\left. + \Theta_3^{\text{out}} \overline{\mathcal{W}}_{1234}^{\text{VRRR}} + \Theta_2^{\text{out}} \Theta_3^{\text{out}} \overline{\mathcal{W}}_{1234}^{\text{RRRR}} \right]. \end{aligned} \quad (38)$$

Inserting the explicit expressions for the various eikonal amplitudes squared and simplifying, we can rewrite (38) in a form analogous to Eqs. (28) and (34):

$$\begin{aligned} \Sigma_{4,\text{ng}}^{\text{ak}_t}(\rho) &= -2 \bar{\alpha}_s^4 \frac{L^4}{4!} \left[C_F C_A^3 \mathcal{G}_{4,a}^{\text{ak}_t}(R) + \right. \\ &\left. + C_F C_A^2 (C_A - 2C_F) \mathcal{G}_{4,b}^{\text{ak}_t}(R) \right], \end{aligned} \quad (39)$$

where, for the first time in the dijet mass distribution, we observe the appearance of a finite- N_c NGLs contribution, namely the term $\mathcal{G}_{4,b}^{\text{ak}_t}$, which is multiplied by the colour factor $(C_A - 2C_F) = 1/N_c$. This colour factor vanishes in the large- N_c limit, i.e., as $N_c \rightarrow \infty$ ³. The NGLs coefficients are given by:

$$\mathcal{G}_{4,a}^{\text{ak}_t}(R) = \mathcal{H}_1 - 3\mathcal{H}_2 - \mathcal{H}_3 + \mathcal{H}_4, \quad (40)$$

where

$$\mathcal{H}_1 = \frac{1}{8} \int_{1_{\text{out}}} \int_{2_{\text{in}}} \int_{3_{\text{in}}} \int_{4_{\text{in}}} \mathcal{A}_{ab}^{12} \mathcal{A}_{ab}^{13} \mathcal{A}_{ab}^{14}, \quad (41a)$$

$$\mathcal{H}_2 = \frac{1}{8} \int_{1_{\text{out}}} \int_{2_{\text{in}}} \int_{3_{\text{out}}} \int_{4_{\text{in}}} \mathcal{A}_{ab}^{12} \mathcal{B}_{ab}^{134}, \quad (41b)$$

$$\mathcal{H}_3 = \frac{1}{8} \int_{1_{\text{out}}} \int_{2_{\text{out}}} \int_{3_{\text{in}}} \int_{4_{\text{in}}} \mathfrak{A}_{ab}^{1234}, \quad (41c)$$

$$\mathcal{H}_4 = \frac{1}{8} \int_{1_{\text{out}}} \int_{2_{\text{out}}} \int_{3_{\text{out}}} \int_{4_{\text{in}}} \mathcal{C}_{ab}^{1234}. \quad (41d)$$

³In practice, the large- N_c limit is achieved by simply setting $C_F \rightarrow C_A/2$.

and

$$\mathcal{G}_{4,b}^{\text{ak}_t}(R) = \frac{1}{8} \int_{1_{\text{out}}} \int_{2_{\text{out}}} \int_{3_{\text{in}}} \int_{4_{\text{in}}} \mathbf{A}_{ab}^{1234}. \quad (42)$$

The various antenna functions are defined in [48]. Performing the integrations, the final results are plotted in Fig. 5. As in previous cases, in the limit $R \rightarrow 0$ we recover the hemisphere mass result [33]: $\mathcal{G}_{4,a}^{\text{ak}_t} = 29\zeta_4/8$ and $\mathcal{G}_{4,b}^{\text{ak}_t} = -\zeta_4/2$.

4 Fixed-order calculations in k_t

This section is devoted to calculations of the dijet mass distribution when final-state jets are defined using the k_t clustering algorithm. As previously stated, the influence of various jet algorithms emerges at two-loops. Thus, at one-loop, this distribution is identical to that of the anti- k_t algorithm, as given in Eq. (18). As is well established, k_t clustering introduces a new tower of clustering logarithms (CLs) for primary emissions while also reducing the magnitude of non-global logarithms (NGLs) for secondary correlated emissions. Therefore, at each loop-order, up to four-loops, we will compute both types of logarithms.

The work presented below builds on the findings of the recently published paper [50], in which the fixed-order analytical structure of the k_t clustering was determined to all-loop orders in the perturbative expansion.

4.1 Two-loops

For the emission of two soft, energy-ordered gluons, k_1 and k_2 , the sum over all possible gluon configurations of the corresponding eikonal amplitudes squared in Eq. (9), with k_t clustering turned on, is given by [50] (see Eq. (16)):

$$\sum_X \hat{\mathcal{U}}_2 \mathcal{W}_{12}^X = -\Theta_1^p \Theta_2^p \Theta_2^{\text{in}} \left[\mathcal{W}_{12}^{\text{VR}} + \Theta_1^{\text{out}} \bar{\Omega}_{12} \mathcal{W}_{12}^{\text{RR}} \right], \quad (43)$$

where $\Omega_{ij} = \Theta(d_{jB} - d_{ij})$ and $\bar{\Omega}_{ij} = 1 - \Omega_{ij}$, with d_{jB} and d_{ij} defined as distance measures in Sec. 2. Notice that if $\Omega_{12} = 0$ (and hence $\bar{\Omega}_{12} = 1$), the above equation reduces to its anti- k_t counterpart, Eq. (21). Using the complementarity relations $\Omega_2^{\text{in}} + \Omega_2^{\text{out}} = 1$ and $\Omega_{12} + \bar{\Omega}_{12} = 1$, substituting for the eikonal amplitudes squared, and simplifying, Eq. (43) reduces to:

$$\begin{aligned} \sum_X \hat{\mathcal{U}}_2 \mathcal{W}_{12}^X &= -\Theta_1^p \Theta_2^p \left[-\Theta_1^{\text{in}} \Theta_2^{\text{in}} \mathcal{W}_1^{\text{R}} \mathcal{W}_2^{\text{R}} - \right. \\ &\left. - \Theta_1^{\text{out}} \Theta_2^{\text{in}} \Omega_{12} \mathcal{W}_1^{\text{R}} \mathcal{W}_2^{\text{R}} + \Theta_1^{\text{out}} \Theta_2^{\text{in}} \bar{\Omega}_{12} \overline{\mathcal{W}}_{12}^{\text{RR}} \right]. \end{aligned} \quad (44)$$

The first term on the rhs corresponds to the case of the anti- k_t (no clustering) algorithm (identical to the first term in Eq. (22)), and is fully accounted for by the exponentiation of the one-loop result (the Sudakov form factor). Indeed, terms

originating from the expansion of the Sudakov form factor appear at every loop order even for the k_t clustering algorithm.

The second term in Eq. (44) represents the new CLs contribution at this order. The corresponding clustering function can be readily identified as:

$$\Xi_{2,\text{cl}}^{\text{kt}}(k_1, k_2) = \Theta_1^{\text{out}} \Theta_2^{\text{in}} \Omega_{12}. \quad (45)$$

This result is identical to those found in, for instance, [25, 26, 39, 43]. Note that if no clustering occurs, that is, if $\Omega_{12} = 0$, CLs are absent. Substituting back into the cumulant expression (9) for $m = 2$, we find the CLs contribution:

$$\Sigma_{2,\text{cl}}^{\text{kt}}(\rho) = \int_{1_{\text{out}}} \int_{2_{\text{in}}} \mathcal{W}_1^R \mathcal{W}_2^R \Omega_{12} = 2 \bar{\alpha}_s^2 \frac{L^2}{2!} C_F^2 \mathcal{F}_2(R), \quad (46)$$

where the factor of 2 accounts for the two jets, $L = \ln(1/\rho)$, and the two-loops CLs coefficient is given by:

$$\mathcal{F}_2(R) = \int_{-c_R}^{c_R} dc_1 \int_{c_R}^1 dc_2 \int_0^{2\pi} \frac{d\phi_1}{2} \int_0^{2\pi} \frac{d\phi_2}{2\pi} w_{ab}^1 w_{ab}^2 \Omega_{12}, \quad (47)$$

where the k_t clustering condition factor, Ω_{12} , is given explicitly by: $\Omega_{12} = \Theta(c_1 c_2 + s_1 s_2 \cos \phi_{12} - c_2)$. The result of the numerical integration is shown in Fig. 2 (A). Notice that as $R \rightarrow 0$, we recover previously reported results [25, 26, 39, 43], with $\mathcal{F}_2(R \sim 0) = 0.183$. This is the *edge* or *boundary* effect observed also in (non-Abelian) NGLs, arising because the corresponding eikonal amplitude is most singular when the two gluons are close to each other. Thus, CLs and NGLs originate chiefly from the boundary of the measured jet [26, 27]. Additionally, from Fig. 2, we observe that the CLs coefficient increases steadily to approximately $R = 1.2$, then falls off towards zero. This may be attributed to the fact that the inter-jet region available for harder emissions decreases as jet radii increase.

The third term in Eq. (44) represents the NGLs contribution. The corresponding clustering function reads:

$$\Xi_{2,\text{ng}}^{\text{kt}}(k_1, k_2) = \Theta_1^{\text{out}} \Theta_2^{\text{in}} \bar{\Omega}_{12}. \quad (48)$$

Notably, unlike CLs, NGLs do not vanish in the case of no clustering (i.e., if $\bar{\Omega}_{12} = 1$); instead, they reduce to the anti- k_t case. Substituting for the irreducible eikonal amplitude, the NGLs contribution to the dijet mass cumulant is:

$$\Sigma_{2,\text{ng}}^{\text{kt}}(\rho) = -2 \bar{\alpha}_s^2 \frac{L^2}{2!} C_F C_A \mathcal{G}_2^{\text{kt}}(R), \quad (49)$$

where the two-loops NGLs coefficient is given by an expression analogous to that of the anti- k_t case (29), but with the integrand multiplied by the clustering condition factor $\bar{\Omega}_{12}$:

$$\mathcal{G}_2^{\text{kt}}(R) = \frac{1}{2} \int_{1_{\text{out}}} \int_{2_{\text{in}}} \mathcal{A}_{ab}^{12} \bar{\Omega}_{12}. \quad (50)$$

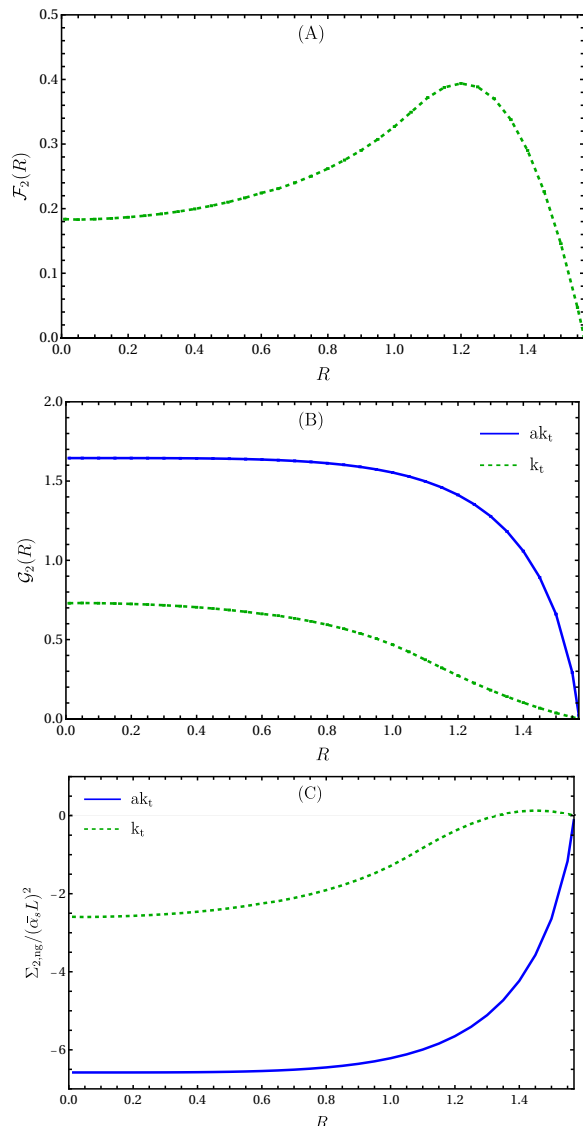


Fig. 2 The two-loops coefficients for CLs (A) and NGLs in both anti- k_t (ak_t) and k_t algorithms (B). A comparison between the NGLs and CLs+NGLs contributions to the dijet mass cumulant at two-loops in anti- k_t and k_t algorithms, respectively (C).

The results as a function of jet-radius R are shown in Fig. 2 (B). We observe that the anti- k_t NGLs coefficient is reduced by more than half due to k_t clustering across the range of jet radii. Note that both NGLs coefficients tend to zero as $R \rightarrow \pi/2$, due to the decreasing phase space for harder emissions.

Comparing the full NGLs contribution (divided by $(\bar{\alpha}_s L)^2$) in the anti- k_t algorithm, Eq. (28), with that in the k_t algorithm, which includes both CLs and NGLs, Eqs. (46) and (49), we see in Fig. 2 (C) that the anti- k_t contribution is reduced by a factor of 2.5 for small values of R , with significantly higher reductions for $R > 0.7$. This confirms previous findings [26, 27], which suggest that using the k_t algorithm with an optimal jet-radius can substantially mitigate NGLs effects on non-global observables. Consequently, the

primary Sudakov form factor serves as a good approximation to the all-orders resummed result for such observables, thus avoiding the intricate task of resumming NGLs.

The dijet mass distribution for the k_t jet algorithm can thus be expressed at two-loops as:

$$\Sigma_2^{k_t}(\rho) = \frac{1}{2!} (\Sigma_1^p)^2 + \Sigma_{2,\text{cl}}^{k_t} + \Sigma_{2,\text{ng}}^{k_t}. \quad (51)$$

Finally, we compare the above result with the output from the fixed-order MC program `event2` for all three colour channels. Specifically, we plot in Fig. 3 the difference (30) for the choice $R = 0.7$. For large (negative) values of the logarithm L , this difference tends to a constant, indicating perfect cancellation of all logarithmic terms. In the $C_F T_f n_f$ channel, k_t clustering has no effect at SL accuracy, which is why the two curves in Fig. 3 for this channel coincide. However, it does have an impact beyond SL, as shown in [21, 27].

In the following section, we present calculations of both CLs and NGLs at three loops in the k_t algorithm. Notably, calculations of the NGLs component at this order have only recently appeared [34] for the dijet azimuthal decorrelation observable. To the best of our knowledge, no similar calculations exist in the current literature.

4.2 Three-loops

The sum over all possible gluon configurations for the emission of three soft, energy-ordered gluons is given by [50]:

$$\begin{aligned} \sum_X \hat{\mathcal{U}}_3 \mathcal{W}_{123}^X &= -\Theta_1^p \Theta_2^p \Theta_3^p \Theta_3^{\text{in}} \left[\mathcal{W}_{123}^{\text{VVR}} + \Theta_1^{\text{out}} \bar{\Omega}_{13} \mathcal{W}_{123}^{\text{RVR}} + \right. \\ &\quad \left. + \Theta_2^{\text{out}} \bar{\Omega}_{23} \mathcal{W}_{123}^{\text{VRR}} + \Theta_1^{\text{out}} \left(\Theta_2^{\text{out}} + \Theta_2^{\text{in}} \Omega_{12} \right) \mathcal{W}_{123}^{\text{RRR}} \right]. \end{aligned} \quad (52)$$

Note that in the absence of clustering ($\Omega_{ij} = 0$ for any pair of gluons (ij)), the above equation reduces to the anti- k_t case, Eq. (31). Following the same steps outlined for the two-loops calculations in the k_t algorithm, we may express the full dijet mass distribution at three-loops as:

$$\Sigma_3^{k_t}(\rho) = \frac{1}{3!} (\Sigma_1^p)^3 + \Sigma_1^p \times \left(\Sigma_{2,\text{cl}}^{k_t} + \Sigma_{2,\text{ng}}^{k_t} \right) + \Sigma_{3,\text{cl}}^{k_t} + \Sigma_{3,\text{ng}}^{k_t}. \quad (53)$$

The first term on the rhs arises from the Sudakov form factor expansion, while the second term represents an interference term between the one-loop primary emissions contribution, Eq. (18), and the two-loops CLs and NGLs contributions, Eqs. (46) and (49), respectively. The third term is the new CLs contribution at this order, expressible in a form analogous to the two-loops result (46):

$$\Sigma_{3,\text{cl}}^{k_t}(\rho) = -2 \bar{\alpha}_s^3 \frac{L^3}{3!} C_F^3 \mathcal{F}_3(R), \quad (54)$$

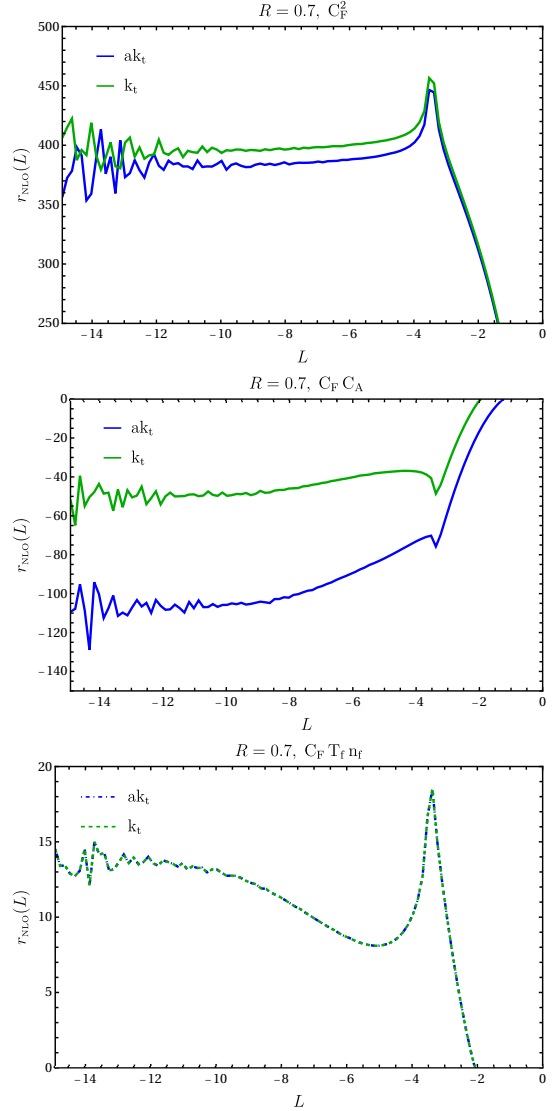


Fig. 3 Comparisons between the analytical and `event2` differential distributions for the dijet mass observable at two-loops for jet-radius $R = 0.7$.

where the three-loops CLs coefficient is given by:

$$\begin{aligned} \mathcal{F}_3(R) &= \left[\int_{1_{\text{out}}} \int_{2_{\text{out}}} \int_{3_{\text{in}}} \Omega_{13} \Omega_{23} \right. \\ &\quad \left. + \int_{1_{\text{out}}} \int_{2_{\text{in}}} \int_{3_{\text{in}}} \Omega_{12} (-1 + \bar{\Omega}_{13} \bar{\Omega}_{23}) \right] w_{ab}^1 w_{ab}^2 w_{ab}^3. \end{aligned} \quad (55)$$

The result of this integration is plotted in Fig. 4 (A). Notice that \mathcal{F}_3 is negative over the entire range of R , which makes the CLs contribution in Eq. (54) positive. In the limit $R \rightarrow 0$, this result converges with that in [43] for the single-jet-mass observable, $\mathcal{F}_3(R \sim 0) = -0.052$. The general features observed at two-loops are retained at three-loops, particularly the boundary nature of CLs and the fall-off to zero at large

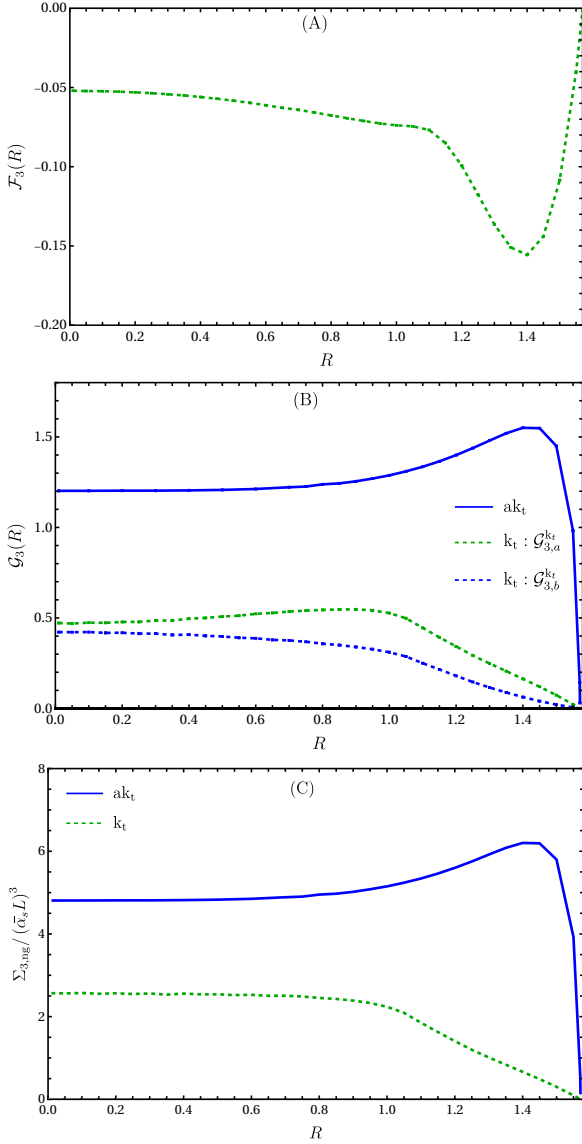


Fig. 4 The three-loop coefficients for CLs (A) and NGLs in both anti- k_t (ak_t) and k_t algorithms (B). A comparison between the NGLs and CLs+NGLs contributions to the dijet mass cumulant at three loops in anti- k_t and k_t algorithms, respectively (C).

R values. Additionally, the magnitude of \mathcal{F}_3 is smaller than that of \mathcal{F}_2 for all values of R , which ensures convergence of the CLs series.

The fourth term in Eq. (53) represents the new NGLs contribution at three-loops, and may be written as:

$$\Sigma_{3,\text{ng}}^{\text{kt}}(\rho) = +2\bar{\alpha}_s^3 \frac{L^3}{3!} \left[C_{\text{F}}^2 C_{\text{A}} \mathcal{G}_{3,a}^{\text{kt}}(R) + C_{\text{F}} C_{\text{A}}^2 \mathcal{G}_{3,b}^{\text{kt}}(R) \right], \quad (56)$$

where the two parts of the NGLs coefficient are given by:

$$\begin{aligned} \mathcal{G}_{3,a}^{\text{kt}}(R) = & \frac{1}{2} \left[\int_{1_{\text{out}}} \int_{2_{\text{out}}} \int_{3_{\text{in}}} \left(\bar{\Omega}_{13} \bar{\Omega}_{23} w_{ab}^1 \mathcal{A}_{ab}^{23} + \bar{\Omega}_{13} \bar{\Omega}_{23} \times \right. \right. \\ & \left. \left. \times [w_{ab}^2 \mathcal{A}_{ab}^{13} + w_{ab}^3 \mathcal{A}_{ab}^{12}] \right) - \right. \\ & \left. - \int_{1_{\text{out}}} \int_{2_{\text{in}}} \int_{3_{\text{in}}} \left(\bar{\Omega}_{12} \bar{\Omega}_{13} \bar{\Omega}_{23} [w_{ab}^1 \mathcal{A}_{ab}^{23} + w_{ab}^2 \mathcal{A}_{ab}^{13}] + \right. \right. \\ & \left. \left. + (\bar{\Omega}_{13} + \bar{\Omega}_{12} (-1 + \bar{\Omega}_{13} \bar{\Omega}_{23})) w_{ab}^3 \mathcal{A}_{ab}^{12} \right) \right], \quad (57a) \end{aligned}$$

and

$$\begin{aligned} \mathcal{G}_{3,b}^{\text{kt}}(R) = & \frac{1}{4} \left[\int_{1_{\text{out}}} \int_{2_{\text{out}}} \int_{3_{\text{in}}} \left(\bar{\Omega}_{13} \bar{\Omega}_{23} \mathcal{A}_{ab}^{12} \bar{\mathcal{A}}_{ab}^{13} \right. \right. \\ & \left. \left. - \bar{\Omega}_{13} \bar{\Omega}_{23} \mathcal{B}_{ab}^{123} \right) + \right. \\ & \left. + \int_{1_{\text{out}}} \int_{2_{\text{in}}} \int_{3_{\text{in}}} \left(\bar{\Omega}_{13} (1 - \bar{\Omega}_{12} \bar{\Omega}_{23}) \mathcal{A}_{ab}^{12} \bar{\mathcal{A}}_{ab}^{13} - \right. \right. \\ & \left. \left. - \bar{\Omega}_{12} \bar{\Omega}_{13} \bar{\Omega}_{23} \mathcal{B}_{ab}^{123} \right) \right]. \quad (57b) \end{aligned}$$

The integration results for both terms are shown in Fig. 4 (B). Several points are noteworthy regarding this contribution:

- The k_t clustering affects both the $C_{\text{F}}^2 C_{\text{A}}$ and $C_{\text{F}} C_{\text{A}}^2$ colour channels, as well as the primary emissions channel (C_{F}^3). Therefore, clustering impacts all colour channels and types of emissions (primary, secondary, and their interferences). Note that in the anti- k_t algorithm, there are no NGLs in the $C_{\text{F}}^2 C_{\text{A}}$ colour channel.
- Both NGLs parts, $\mathcal{G}_{3,a}^{\text{kt}}$ and $\mathcal{G}_{3,b}^{\text{kt}}$, are smaller in magnitude than the anti- k_t counterpart $\mathcal{G}_3^{\text{akt}}$, reduced by more than half across the range of R . The term $\mathcal{G}_{3,b}^{\text{kt}}$ (blue dashed curve in (B)) corresponds to the reduction in the anti- k_t NGLs coefficient $\mathcal{G}_3^{\text{kt}}$ due to k_t clustering, as they both share the same colour factor.
- The combined effect of both primary and secondary emissions in k_t clustering again reduces the overall impact of anti- k_t NGLs, as shown in Fig. 4 (C). The reduction is approximately 50%, dominated by $\mathcal{G}_{3,b}^{\text{kt}}$ due to its large colour factor ($C_{\text{F}} C_{\text{A}}^2$).
- The clustering functions for both primary, $\bar{\Sigma}_{3,\text{cl}}^{\text{kt}}$, and secondary, $\bar{\Sigma}_{3,\text{ng}}^{\text{kt}}$, emissions can be inferred from Eq. (52) upon substitution of the explicit eikonal amplitudes squared. However, we do not present them explicitly here as they are quite cumbersome. The CLs and NGLs coefficients in Eqs. (55), (57a), and (57b) include only parts of these clustering functions, excluding interference terms with lower orders.

The next section presents calculations with k_t clustering at four-loops. Unlike CLs, for which similar calculations exist

in the literature [39, 43], NGLs at this loop-order are unique to this work and have not previously appeared in the literature.

4.3 Four-loops

The four-loop calculations follow the same procedural steps as those established in previous lower loop orders. The sum over all possible gluon configurations of the squared eikonal amplitudes, in Eq. (9) for $m = 4$, is given in Eq. (20) of Ref. [50]:

$$\begin{aligned} \sum_X \hat{\mathcal{U}}_4 \mathcal{W}_{1234}^X &= -\Theta_1^p \Theta_2^p \Theta_3^p \Theta_4^p \Theta_4^{\text{in}} \left[\mathcal{W}_{1234}^{\text{VVVR}} + \Theta_1^{\text{out}} \bar{\Omega}_{14} \mathcal{W}_{1234}^{\text{RVVR}} + \right. \\ &+ \Theta_2^{\text{out}} \bar{\Omega}_{24} \mathcal{W}_{1234}^{\text{VRVR}} + \Theta_3^{\text{out}} \bar{\Omega}_{34} \mathcal{W}_{1234}^{\text{VRRR}} + \\ &+ \Theta_1^{\text{out}} \left(\Theta_2^{\text{out}} + \Theta_2^{\text{in}} \Omega_{12} \right) \bar{\Omega}_{14} \bar{\Omega}_{24} \mathcal{W}_{1234}^{\text{RRVR}} \\ &+ \Theta_1^{\text{out}} \left(\Theta_3^{\text{out}} + \Theta_3^{\text{in}} \Omega_{13} \right) \bar{\Omega}_{14} \bar{\Omega}_{34} \mathcal{W}_{1234}^{\text{RVRR}} \\ &+ \Theta_2^{\text{out}} \left(\Theta_3^{\text{out}} + \Theta_3^{\text{in}} \Omega_{23} \right) \bar{\Omega}_{24} \bar{\Omega}_{34} \mathcal{W}_{1234}^{\text{VRRR}} \\ &+ \Theta_1^{\text{out}} \left(\Theta_2^{\text{out}} + \Theta_2^{\text{in}} \Omega_{12} \right) \times \\ &\times \left(\Theta_3^{\text{out}} + \Theta_3^{\text{in}} \left[\Omega_{23} + \bar{\Omega}_{23} \Omega_{13} \right] \right) \bar{\Omega}_{14} \bar{\Omega}_{24} \bar{\Omega}_{34} \times \\ &\left. \mathcal{W}_{1234}^{\text{RRRR}} \right]. \end{aligned} \quad (58)$$

Some of the important features and symmetry patterns of this formula are discussed in Ref. [50]. Notice that, in the absence of clustering, the equation above reduces to Eq. (36) of the anti- k_t case. Upon substituting the expressions for the various squared eikonal amplitudes, we obtain the four-loop cumulant (9):

$$\begin{aligned} \Sigma_4^{\text{kt}}(\rho) &= \frac{1}{4!} \left(\Sigma_1^{\text{p}} \right)^4 + \Sigma_1^{\text{p}} \times \left(\Sigma_{3,\text{cl}}^{\text{kt}} + \Sigma_{3,\text{ng}}^{\text{kt}} \right) + \\ &+ \frac{1}{2!} \left(\Sigma_1^{\text{p}} \right)^2 \times \left(\Sigma_{2,\text{cl}}^{\text{kt}} + \Sigma_{2,\text{ng}}^{\text{kt}} \right) + \frac{1}{2!} \left(\Sigma_{2,\text{cl}}^{\text{kt}} \right)^2 + \\ &+ \frac{1}{2!} \left(\Sigma_{2,\text{ng}}^{\text{kt}} \right)^2 + \Sigma_{4,\text{cl}}^{\text{kt}} + \Sigma_{4,\text{ng}}^{\text{kt}}. \end{aligned} \quad (59)$$

The last two terms represent the new CLs and NGLs contributions at this order. The CLs term, $\Sigma_{4,\text{cl}}^{\text{kt}}$, may be cast, as usual, in the form:

$$\Sigma_{4,\text{cl}}^{\text{kt}}(\rho) = +2 \bar{\alpha}_s^4 \frac{L^4}{4!} C_{\text{F}}^4 \mathcal{F}_4(R), \quad (60)$$

where the CLs four-loop coefficient has the explicit expression:

$$\begin{aligned} \mathcal{F}_4(R) &= \left[\int_{1_{\text{out}}} \int_{2_{\text{out}}} \int_{3_{\text{out}}} \int_{4_{\text{in}}} \Omega_{14} \Omega_{24} \Omega_{34} \right. \\ &+ \int_{1_{\text{out}}} \int_{2_{\text{out}}} \int_{3_{\text{in}}} \int_{4_{\text{in}}} \left[\Omega_{13} \Omega_{24} (-1 + \bar{\Omega}_{14} \bar{\Omega}_{34}) + \Omega_{23} \times \right. \\ &\times \left. \left. \left(-\Omega_{13} - \Omega_{14} + \bar{\Omega}_{24} \bar{\Omega}_{34} (1 - \bar{\Omega}_{13} \bar{\Omega}_{14}) \right) \right] \right. \\ &+ \int_{1_{\text{out}}} \int_{2_{\text{in}}} \int_{3_{\text{out}}} \int_{4_{\text{in}}} \Omega_{12} \Omega_{34} (-1 + \bar{\Omega}_{14} \bar{\Omega}_{24}) \\ &+ \int_{1_{\text{out}}} \int_{2_{\text{in}}} \int_{3_{\text{in}}} \int_{4_{\text{in}}} \Omega_{12} (-1 + \bar{\Omega}_{13} \bar{\Omega}_{23}) \times \\ &\left. \times \left(-1 + \bar{\Omega}_{14} \bar{\Omega}_{24} \bar{\Omega}_{34} \right) \right] w_{ab}^1 w_{ab}^2 w_{ab}^3 w_{ab}^4. \end{aligned} \quad (61)$$

The results of the integration are plotted in Fig. 5 (A). For small values of the jet radius R , one recovers the value reported in [43], specifically $\mathcal{F}_4(R \sim 0) = 0.0226$.

Similarly, the NGLs term at this order can be expressed as:

$$\begin{aligned} \Sigma_{4,\text{ng}}^{\text{kt}}(\rho) &= -2 \bar{\alpha}_s^2 \frac{L^4}{4!} \left[-C_{\text{F}}^3 C_{\text{A}} \mathcal{G}_{4,a}^{\text{kt}} - C_{\text{F}}^2 C_{\text{A}}^2 \mathcal{G}_{4,b}^{\text{kt}} + \right. \\ &\left. + C_{\text{F}} C_{\text{A}}^3 \mathcal{G}_{4,c}^{\text{kt}} + C_{\text{F}} C_{\text{A}}^2 (C_{\text{A}} - 2C_{\text{F}}) \mathcal{G}_{4,d}^{\text{kt}} \right], \end{aligned} \quad (62)$$

where the expressions of the various NGLs terms are complex, and we refrain from showing them explicitly. The final integration results are displayed in Fig. 5 ((B) and (C)) as a function of the jet radius R . Notably, both $C_{\text{F}} C_{\text{A}}^3$ and finite- N_c coefficients, $\mathcal{G}_{4,c}^{\text{kt}}$ and $\mathcal{G}_{4,d}^{\text{kt}}$ in the equation above, are negative, and a minus sign has been extracted from the former, $\mathcal{G}_{4,c}^{\text{kt}}$, to maintain analogy with the anti- k_t case ($\Sigma_{4,\text{ng}}^{\text{akt}}$ in Eq. (39)). All characteristics observed at lower orders persist at four-loop order, including that k_t clustering affects all colour channels and that the dominant contribution arises from the term associated with the largest colour factor ($C_{\text{F}} C_{\text{A}}^3$). The NGLs reduction due to clustering at this order exceeds 50% across all values of the jet-radius, as demonstrated in Fig. 5 (D).

4.4 Exponentiation

The calculations of the dijet mass distribution in both anti- k_t and k_t jet algorithms up to four-loops, Eqs. (25), (32), (37), (51), (53), and (59), clearly indicate a pattern of exponentiation for both CLs and NGLs. The latter may be expressed as [33, 43]:

$$\mathcal{S}^{\text{JA}}(\rho) = \exp \left[-2 \sum_{n \geq 2} \frac{1}{n!} \mathcal{S}_n^{\text{JA}}(R) (-\bar{\alpha}_s L)^n \right], \quad (63a)$$

$$\mathcal{C}(\rho) = \exp \left[2 \sum_{n \geq 2} \frac{1}{n!} \mathcal{F}_n(R) (-C_{\text{F}} \bar{\alpha}_s L)^n \right], \quad (63b)$$

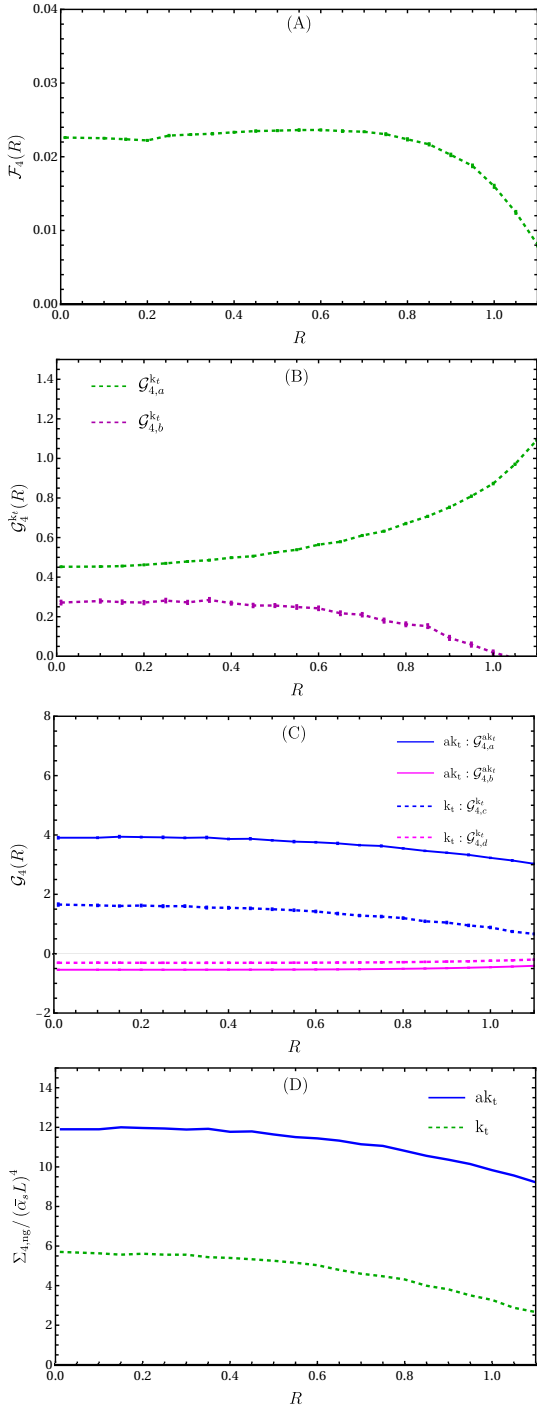


Fig. 5 The four-loop coefficients for CLs (A), NGLs unique to the k_t algorithm (B), and NGLs present in both anti- k_t (ak_t) and k_t algorithms (C). Comparison between NGLs and CLs+NGLs contributions to the dijet mass cumulant at four-loop order in the anti- k_t and k_t algorithms, respectively (D).

where the superscript JA refers to a given jet algorithm, i.e., anti- k_t or k_t , and hence $\mathcal{S}_n^{\text{ak}_t}$, for the anti- k_t , is given by:

$$\begin{aligned} \mathcal{S}_2^{\text{ak}_t} &= C_F C_A \mathcal{G}_2^{\text{ak}_t}, & \mathcal{S}_3^{\text{ak}_t} &= C_F C_A^2 \mathcal{G}_3^{\text{ak}_t}, \\ \mathcal{S}_4^{\text{ak}_t} &= C_F C_A^3 \mathcal{G}_{4,a}^{\text{ak}_t} + C_F C_A^2 (C_A - 2C_F) \mathcal{G}_{4,b}^{\text{ak}_t}, \end{aligned} \quad (64a)$$

and for k_t :

$$\begin{aligned} \mathcal{S}_2^{k_t} &= C_F C_A \mathcal{G}_2^{k_t}, & \mathcal{S}_3^{k_t} &= C_F^2 C_A \mathcal{G}_{3,a}^{k_t} + C_F C_A^2 \mathcal{G}_{3,b}^{\text{ak}_t}, \\ \mathcal{S}_4^{k_t} &= -C_F^3 C_A \mathcal{G}_{4,a}^{k_t} - C_F^2 C_A^2 \mathcal{G}_{4,b}^{k_t} + C_F C_A^3 \mathcal{G}_{4,c}^{\text{ak}_t} + \\ &\quad + C_F C_A^2 (C_A - 2C_F) \mathcal{G}_{4,d}^{k_t}. \end{aligned} \quad (64b)$$

Due to the alternating signs in both the CLs and NGLs series (for both jet algorithms), and to assess their convergence and approximation to the all-orders result, we shall compare the exponentials in Eqs. (63a) and (63b) to the all-orders numerical output of the MC code of [4] in Section 5.1. Although this code computes NGLs in the large- N_c limit, it remains the only available code that implements k_t clustering and accommodates various non-global observables. Finite- N_c MC codes, such as those in [17, 18], are restricted to specific observables (excluding the dijet mass) and lack k_t clustering.

Before conducting these comparisons, we shall first outline, in the next section, the all-orders resummed formula for the dijet mass distribution, incorporating both CLs and NGLs contributions.

5 All-orders resummation

The resummation of large logarithms appearing in the distribution of the dijet mass non-global observable can be cast in the following factorised formula [4, 26]:

$$\Sigma^{\text{JA}}(\rho) = \Sigma^{\text{P}}(\rho) \mathcal{S}^{\text{JA}}(t) \mathcal{C}(t), \quad (65)$$

where Σ^{P} is the well-known Sudakov form factor that resums primary emissions and takes the usual standard form [54]:

$$\Sigma^{\text{P}}(\rho) = \frac{\exp(-\mathcal{R} - \gamma_E \mathcal{R}')}{\Gamma(1 + \mathcal{R}')}, \quad (66)$$

where $\gamma_E = 0.577$ is the Euler–Mascheroni constant, \mathcal{R} , known as the global radiator, is a function of ρ and R^2 that represents the resummation of large global logarithms to NLL accuracy, and \mathcal{R}' is its derivative with respect to the logarithm $L' = \log(R^2/\rho)$. The full expression of this radiator and its derivative can be found in Refs. [25, 27].

The NGLs form factor, $\mathcal{S}^{\text{JA}}(t)$, can be parametrised by the following exponential, initially proposed in [4]:

$$\mathcal{S}_{\text{MC}}^{\text{JA}}(t) = \exp \left[-C_F C_A \mathcal{G}_2^{\text{JA}}(R) \left(\frac{1 + (at)^2}{1 + (bt)^c} \right) t^2 \right], \quad (67)$$

where a , b , and c are fitting parameters to the MC output, $\mathcal{G}_2^{\text{JA}}$ is the two-loop NGLs coefficient for the jet algorithm JA (anti- k_t or k_t), and t is the evolution variable, given at SL accuracy by:

$$t = \frac{1}{2\pi} \int_{\frac{\rho}{R^2}}^1 \frac{dx}{x} \alpha_s(xQ/2) = -\frac{1}{4\pi\beta_0} \ln [1 - 2\alpha_s\beta_0 L'], \quad (68)$$

with $\alpha_s(QR/2)$ and L' defined as above. The CLs form factor assumes an analogous form:

$$\mathcal{C}_{\text{MC}}(t) = \exp \left[C_F^2 \mathcal{F}_2(R) \left(\frac{1 + (at)^2}{1 + (bt)^c} \right) t^2 \right], \quad (69)$$

where \mathcal{F}_2 is the two-loop CLs coefficient in the k_t algorithm. The fitting parameters depend on the jet radius, the jet algorithm, and differ for NGLs and CLs resummations. In Tables 1 and 2, we show the values of the fitting parameters used for the NGLs and CLs parametrisations, respectively.

| Jet algorithm | R | \mathcal{G}_2 | a | b | c |
|---------------|-----|-----------------|------------|------------|------|
| anti- k_t | 0.7 | 6.51 | 0.02 C_A | 0.58 C_A | 1.48 |
| | 1.0 | 6.21 | 0.01 C_A | 0.92 C_A | 1.81 |
| k_t | 0.7 | 2.54 | 0.96 C_A | 0.44 C_A | 0.14 |
| | 1.0 | 1.87 | 0.91 C_A | 2.99 C_A | 0.15 |

Table 1 Values of the fitting parameters for the parametrisation of the NGLs resummed form factor.

| Jet algorithm | R | \mathcal{F}_2 | a | b | c |
|---------------|-----|-----------------|------------|------------|------|
| k_t | 0.7 | 0.96 | 0.57 C_A | 0.72 C_A | 1.62 |
| | 1.0 | 1.31 | 0.19 C_A | 0.25 C_A | 0.42 |

Table 2 Values of the fitting parameters for the parametrisation of the CLs resummed form factor.

The resummed distribution (65) is plotted in Fig. 6 for both anti- k_t and k_t jet algorithms. For $R = 0.7$, the peak of the Sudakov distribution is shifted towards higher values of ρ in the anti- k_t algorithm and is reduced by about 24%. In the k_t algorithm, the position of this peak remains unchanged and is reduced by only 5%. For $R = 1.0$, the same observations hold, with reductions of about 22% and 2% for anti- k_t and k_t algorithms, respectively. Larger values of R would result in even smaller reductions, particularly for the k_t algorithm. These results reinforce previous conclusions [26, 27] that selecting the k_t algorithm over the anti- k_t algorithm has the advantage of minimising the complex effect of NGLs, thereby making the Sudakov primary resummation more reliable.

5.1 Comparisons of analytical and MC results

In this section, we compare the analytical exponentiation of the fixed-order calculations of NGLs and CLs terms, Eqs. (63a) and (63b), with the numerical distributions obtained from the MC of [4], represented by the parametrisations (67) and (69). At fixed-order, $t = \bar{\alpha}_s L'/2$, so we replace $\bar{\alpha}_s L'$ in Eqs. (63a) and (63b) by $2t$. Furthermore, the legends “2loops”, “3loops”

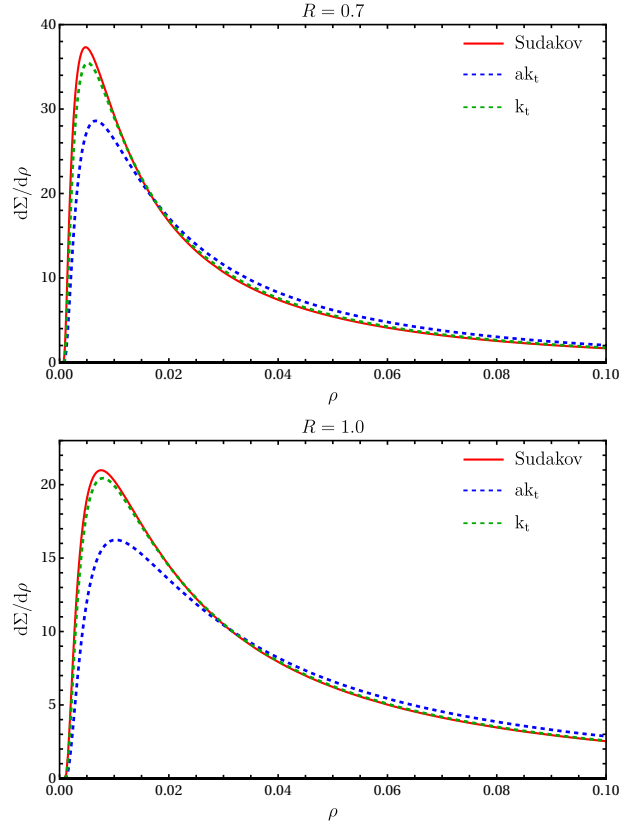


Fig. 6 The resummed distribution for the dijet mass observable (65) with and without the inclusion of NGLs and CLs form factors for both anti- k_t and k_t jet algorithms at $R = 0.7$ and $R = 1.0$.

and “4loops” in Figs. 7, 8, and 9 indicate truncating the series in the exponents of these equations at two-, three-, and four-loops, respectively.

For the anti- k_t jet algorithm, the two-loop NGLs exponential approximates the all-orders NGLs distribution quite well over the entire range of t . The case is less accurate for the k_t algorithm. Adding contributions from higher loop-orders improves the approximation at small (but phenomenologically important) values of t . This is particularly true when up to four-loop terms are included in the exponent of the analytical expressions.

It is worth noting that for comparisons of the CLs distributions (Fig. 9), we used the parametrisation adopted in the MC code [4] and implemented in our previous paper [43] (Eq. (A.8)). In this parametrisation, the numerical values of the CLs coefficients match those found here for small values of R (up to about $R = 0.5$) but are generally slightly lower for larger values. The CL series appears to converge to the all-orders result faster than the NGL series. This is evident from the decreasing (absolute) values of the CL coefficients at higher loop orders, as well as from the “4loops” curve in Fig. 9. Notably, the CL form factor contributes, for $R = 0.7$, up to a maximum of 10% of the resummed primary emis-

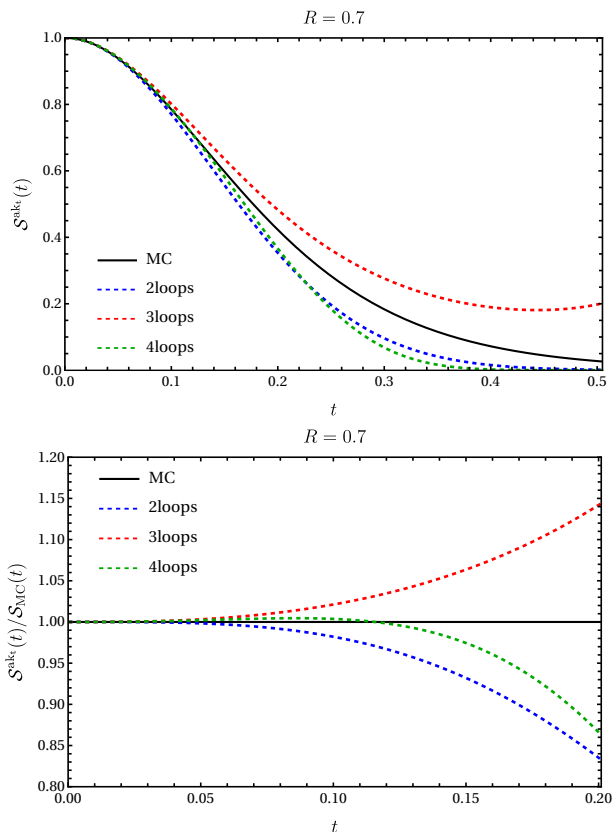


Fig. 7 Comparison between the exponential of fixed-order NGLs results and the output of the MC code from [4] for the anti- k_t algorithm with $R = 0.7$.

sions for values of t up to 0.25. Smaller percentage contributions are observed for smaller values of t .

6 Conclusion

In this paper, we have investigated the fixed-order and all-orders resummed distribution of the normalised invariant mass (squared) observable for dijets produced at threshold in e^+e^- annihilation processes. This observable belongs to the class of non-global observables, which are known for their delicate properties and intricate calculations. Gaining deeper insights and a clearer understanding of their structure has been the subject of numerous studies over the last two decades.

Employing eikonal (soft) theory together with strong-energy ordering of emitted gluons, we have computed the fixed-order distribution of this observable up to four-loops, at single-logarithmic accuracy, for both anti- k_t and k_t jet algorithms. Our analytical results include the full jet-radius and colour dependence. We have derived in detail the complete contributions of both NGLs and CLs and demonstrated how an optimal choice of the jet-radius, in k_t , may lead to the two large logarithms balancing each other out at each order and to all-orders in perturbative expansion. Additionally, we have confirmed many features identified in previous studies,

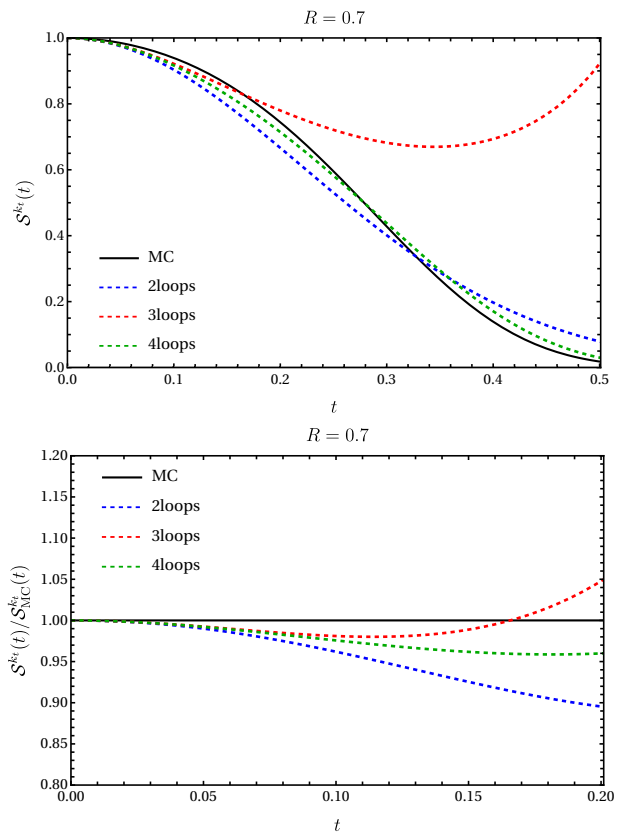


Fig. 8 Comparison between the exponential of fixed-order NGLs results and the output of the MC code from [4] for the k_t algorithm with $R = 0.7$.

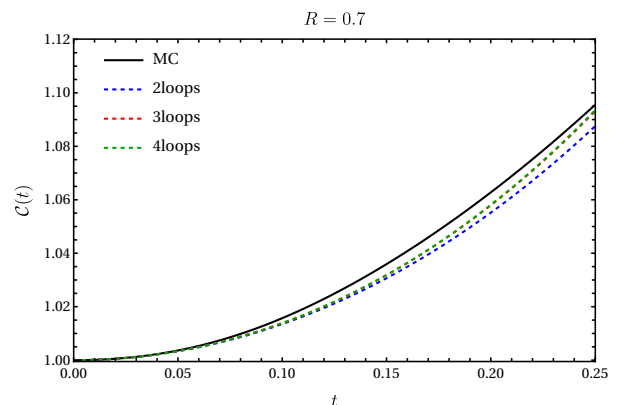


Fig. 9 Comparison between the exponential of fixed-order CLs results and the output of the MC code from [4] for the k_t algorithm with $R = 0.7$.

such as the edge effects of both NGLs and CLs, the impact of large colour factors, and the pattern of exponentiation.

While NGLs and CLs have been addressed in prior studies, the calculations presented here, particularly for the k_t jet algorithm, are distinct in that they allow these logarithms to be determined in a systematic way to any order in perturbation theory (within the above soft and energy-ordering approximations). This is enabled by the recently developed

master formula for the structure of k_t clustering at any order in perturbation theory [50]. For instance, the calculation of the four-loop NGLs coefficient in k_t is presented herein for the first time in the literature.

Moreover, we have derived the all-orders resummed expression for the dijet mass observable up to NLL accuracy, including both NGLs and CLs form factors. The findings align with the fixed-order results, demonstrating that the inclusion of CLs greatly reduces the effect of NGLs, thereby making the Sudakov primary form factor more reliable. This result offers an effective way of avoiding the complexities of NGLs altogether. Additionally, comparisons of the exponentiation of the analytical results with the all-orders output of numerical MC codes reveal noticeable differences between CLs and NGLs distributions. While for CLs, the analytical expression approximates the full all-orders numerical result well over a wide range of observable values, the NGLs approximation holds only for small values of the observable. This observation regarding NGLs is valid for both anti- k_t and k_t jet algorithms.

It is worth investigating the impact of other jet algorithms, such as Cambridge/Aachen, on the distribution of non-global observables at both fixed-order and all-orders in perturbation theory, especially since no corresponding MC codes implement the latter jet algorithm. Furthermore, it may prove useful to extend the current work to more complex QCD environments, such as Deep Inelastic Scattering (DIS) and hadron-hadron collision processes.

References

1. M. Cacciari, G.P. Salam, G. Soyez, *JHEP* **04**, 063 (2008). DOI 10.1088/1126-6708/2008/04/063
2. S. Catani, Y.L. Dokshitzer, M.H. Seymour, B.R. Webber, *Nucl. Phys. B* **406**, 187 (1993). DOI 10.1016/0550-3213(93)90166-M
3. S.D. Ellis, D.E. Soper, *Phys. Rev. D* **48**, 3160 (1993). DOI 10.1103/PhysRevD.48.3160
4. M. Dasgupta, G.P. Salam, *Phys. Lett. B* **512**, 323 (2001). DOI 10.1016/S0370-2693(01)00725-0
5. M. Dasgupta, G.P. Salam, *JHEP* **03**, 017 (2002). DOI 10.1088/1126-6708/2002/03/017
6. A. Gehrmann-De Ridder, T. Gehrmann, E.W.N. Glover, G. Heinrich, *JHEP* **12**, 094 (2007). DOI 10.1088/1126-6708/2007/12/094
7. V. Del Duca, C. Duhr, A. Kardos, G. Somogyi, Z. Szőr, Z. Trócsányi, Z. Tulipánt, *Phys. Rev. D* **94**(7), 074019 (2016). DOI 10.1103/PhysRevD.94.074019
8. A. Banfi, H. McAslan, P.F. Monni, G. Zanderighi, *JHEP* **05**, 102 (2015). DOI 10.1007/JHEP05(2015)102
9. T. Becher, M.D. Schwartz, *JHEP* **07**, 034 (2008). DOI 10.1088/1126-6708/2008/07/034
10. R. Abbate, M. Fickinger, A.H. Hoang, V. Mateu, I.W. Stewart, *Phys. Rev. D* **83**, 074021 (2011). DOI 10.1103/PhysRevD.83.074021
11. Y.T. Chien, M.D. Schwartz, *JHEP* **08**, 058 (2010). DOI 10.1007/JHEP08(2010)058
12. V. Mateu, G. Rodrigo, *JHEP* **11**, 030 (2013). DOI 10.1007/JHEP11(2013)030
13. A.H. Hoang, D.W. Kolodrubetz, V. Mateu, I.W. Stewart, *Phys. Rev. D* **91**(9), 094017 (2015). DOI 10.1103/PhysRevD.91.094017
14. I. Moutl, H.X. Zhu, *JHEP* **08**, 160 (2018). DOI 10.1007/JHEP08(2018)160
15. T. Becher, M. Neubert, *JHEP* **01**, 025 (2020). DOI 10.1007/JHEP01(2020)025
16. A. Banfi, G. Marchesini, G. Smye, *JHEP* **08**, 006 (2002). DOI 10.1088/1126-6708/2002/08/006
17. Y. Hatta, T. Ueda, *Nucl. Phys. B* **874**, 808 (2013). DOI 10.1016/j.nuclphysb.2013.06.021
18. Y. Hagiwara, Y. Hatta, T. Ueda, *Phys. Lett. B* **756**, 254 (2016). DOI 10.1016/j.physletb.2016.03.028
19. Y. Hatta, T. Ueda, *Nucl. Phys. B* **962**, 115273 (2021). DOI 10.1016/j.nuclphysb.2020.115273
20. M. De Angelis, J.R. Forshaw, S. Plätzer, *Phys. Rev. Lett.* **126**(11), 112001 (2021). DOI 10.1103/PhysRevLett.126.112001
21. A. Banfi, F.A. Dreyer, P.F. Monni, *JHEP* **10**, 006 (2021). DOI 10.1007/JHEP10(2021)006
22. T. Becher, N. Schalch, X. Xu, *Phys. Rev. Lett.* **132**(8), 081602 (2024). DOI 10.1103/PhysRevLett.132.081602
23. M. Dasgupta, Y. Delenda, *JHEP* **08**, 080 (2006). DOI 10.1088/1126-6708/2006/08/080
24. A. Banfi, M. Dasgupta, Y. Delenda, *Phys. Lett. B* **665**, 86 (2008). DOI 10.1016/j.physletb.2008.05.065
25. A. Banfi, M. Dasgupta, K. Khelifa-Kerfa, S. Marzani, *JHEP* **08**, 064 (2010). DOI 10.1007/JHEP08(2010)064
26. K. Khelifa-Kerfa, *JHEP* **02**, 072 (2012). DOI 10.1007/JHEP02(2012)072
27. K.K. Kerfa, QCD resummation for high- p_T jet shapes at hadron colliders. Ph.D. thesis, Manchester U. (2012)
28. M. Dasgupta, K. Khelifa-Kerfa, S. Marzani, M. Spannowsky, *JHEP* **10**, 126 (2012). DOI 10.1007/JHEP10(2012)126
29. H. Bouaziz, Y. Delenda, K. Khelifa-Kerfa, *JHEP* **10**, 006 (2022). DOI 10.1007/JHEP10(2022)006
30. M.D. Schwartz, H.X. Zhu, *Phys. Rev. D* **90**(6), 065004 (2014). DOI 10.1103/PhysRevD.90.065004
31. S. Caron-Huot, (2015). private communication
32. H. Benslama, Y. Delenda, K. Khelifa-Kerfa, A.M. Ibrahim, *Phys. Part. Nucl. Lett.* **18**(1), 5 (2021). DOI 10.1134/S1547477121010039
33. K. Khelifa-Kerfa, Y. Delenda, *JHEP* **03**, 094 (2015). DOI 10.1007/JHEP03(2015)094

-
34. H. Benslama, Y. Delenda, K. Khelifa-Kerfa, Phys. Lett. B **840**, 137903 (2023). DOI 10.1016/j.physletb.2023.137903
 35. K. Khelifa-Kerfa, (2024). DOI 10.1007/JHEP10(2024)079
 36. R.B. Appleby, M.H. Seymour, JHEP **12**, 063 (2002). DOI 10.1088/1126-6708/2002/12/063
 37. R.B. Appleby, M.H. Seymour, JHEP **09**, 056 (2003). DOI 10.1088/1126-6708/2003/09/056
 38. A. Banfi, M. Dasgupta, Phys. Lett. **B628**, 49 (2005). DOI 10.1016/j.physletb.2005.08.125
 39. Y. Delenda, R. Appleby, M. Dasgupta, A. Banfi, JHEP **0612**, 044 (2006). DOI 10.1088/1126-6708/2006/12/044
 40. R. Kelley, J.R. Walsh, S. Zuberi, JHEP **09**, 117 (2012). DOI 10.1007/JHEP09(2012)117
 41. R. Kelley, J.R. Walsh, S. Zuberi, (2012)
 42. N. Ziani, K. Khelifa-Kerfa, Y. Delenda, Eur. Phys. J. C **81**, 570 (2021). DOI 10.1140/epjc/s10052-021-09379-z
 43. Y. Delenda, K. Khelifa-Kerfa, JHEP **09**, 109 (2012). DOI 10.1007/JHEP09(2012)109
 44. K. Khelifa-Kerfa, NGLs up to four-loops for V/H+jet processes in k_t algorithm. in progress
 45. Y.L. Dokshitzer, G.D. Leder, S. Moretti, B.R. Webber, JHEP **08**, 001 (1997). DOI 10.1088/1126-6708/1997/08/001
 46. M. Wobisch, T. Wengler, in *Workshop on Monte Carlo Generators for HERA Physics (Plenary Starting Meeting)* (1998), pp. 270–279
 47. T. Becher, J. Haag, JHEP **01**, 155 (2024). DOI 10.1007/JHEP01(2024)155
 48. Y. Delenda, K. Khelifa-Kerfa, Phys. Rev. D **93**(5), 054027 (2016). DOI 10.1103/PhysRevD.93.054027
 49. R. Kelley, M.D. Schwartz, H.X. Zhu, (2011)
 50. K. Khelifa-Kerfa, (2024)
 51. S. Catani, M.H. Seymour, Phys. Lett. **B378**, 287 (1996). DOI 10.1016/0370-2693(96)00425-X
 52. M. Cacciari, G.P. Salam, G. Soyez, Eur. Phys. J. C **72**, 1896 (2012). DOI 10.1140/epjc/s10052-012-1896-2
 53. M. Cacciari, G.P. Salam, Phys. Lett. **B641**, 57 (2006). DOI 10.1016/j.physletb.2006.08.037
 54. S. Catani, L. Trentadue, G. Turnock, B.R. Webber, Nucl. Phys. **B407**, 3 (1993). DOI 10.1016/0550-3213(93)90271-P